Two unconventional precursors to produce $ZnCl_2$-based activated carbon for water treatment applications

Gerardo Juan Francisco Cruz[1,*], Minna Pirilä[2], Lenka Matějová[3,4], Kaisu Ainassaari[2], Jose Luis Solis[5], Radek Fajgar[3], Olga Šolcová[3], Riitta Liisa Keiski[2]

[1] Universidad Nacional de Tumbes, Facultad de Ciencias Agrarias, Laboratorio de Análisis Ambiental, Av. Universitaria s/n, Campus Universitario – Pampa Grande, Tumbes, Perú

[2] University of Oulu, Faculty of Technology, Environmental and Chemical Engineering, P.O. Box 4300, FI-90014, Finland

[3] Institute of Chemical Process Fundamentals of the CAS, v. v. i., Rozvojová 135, CZ-165 02 Prague, Czech Republic

[4] Institute of Environmental Technology, VŠB – Technical University of Ostrava, 17. listopadu 15/2172, CZ-708 00 Ostrava-Poruba, Czech Republic

[5] Universidad Nacional de Ingeniería, Facultad de Ciencias, Laboratorio de Materiales Funcionales, Av. Tupac Amaru 210, Lima 25, Perú

*Correspondence: Gerardo Juan Francisco Cruz (E-mail: gcruzc@untumbes.edu.pe), Universidad Nacional de Tumbes, Facultad de Ciencias Agrarias, Laboratorio de Análisis Ambiental, Av. Universitaria s/n, Campus Universitario – Pampa Grande, Tumbes, Perú

Abstract

Two unconventional raw materials, the seeds from *Spondias purpurea* L. (red mombin) and *Inga edulis* (ice cream-bean), were characterized and used as precursors to produce good quality Zinc Chloride-activated carbons for potential use in water treatment applications. Red Mombin seed was significantly more porous than ice cream bean seed, while the activated carbons prepared from red mombin seed and ice cream-bean seeds showed both a very well-established microporous-mesoporous structure. Equilibrium as well as kinetic adsorption experiments were conducted with methylene blue, methyl orange and As(V). It was revealed that both seeds are unconventional, renewable, cheap and suitable agro-precursors for production of activated carbons with potential application in wastewater treatment.

Keywords: Activated carbon**;** Adsorption; Biomass; Dyes; Heavy metals

1 Introduction

Two promising species of trees from the tropical forest, because of their current and potential uses, are *Spondias purpurea* L. (Anacardiaceae) and *Inga edulis* (Leguminosae: Mimosoideae). The *Spondias purpurea* L. fruit is edible and it is commonly known in different countries as red mombin, purple mombin, plum, hog plum, *jocote*, *sineguela*, *sireguela*, *ciruela* and *jocote corona*. On the other hand, the common names for *I. edulis* are ice-cream bean tree, *guaba*, *guabo*, *guamo bejuco*, *guano*, *huaba*, *inga* and *rabo de mico*. Both raw materials contain seeds, which are a significant proportion of the whole fruit and currently they are disposed as residues with the negative

Received: March 29, 2018; revised: April 25, 2018; accepted: May 25, 2018

To be cited as: Chem. Eng. Technol. 10.1002/ceat.201800150

Link to final VoR: https://doi.org/10.1002/ceat.201800150

environmental concerns that it involves: air and soil pollution, landscape changes among others. Those seeds, as all materials with a similar nature, contain cellulose, hemicellulose and lignin and thus could be used in the production of activated carbon (AC), a product with high aggregate value, widely utilized as an adsorbent material for water and wastewater treatment. Currently, coal is the major starting material to produce AC, however it is relatively expensive, non-renewable and a highly structured material that could be used for energy generation instead of pollution control applications [1] [2]. Therefore, it is important to find new low-cost, renewable materials to replace the conventional AC precursors. Agricultural by-products are suitable feedstocks for the AC production, based on their availability as renewable resources, low ash content, reasonable hardness and their ability to produce AC with high adsorption capacity [3]. Some seeds have been studied as starting materials for the AC production to be specifically used in environmental applications: avocado kernel seed [4], cherry stone [5], grape seed [6, 7], sour cherry stone [8], olive stone [9], pomegranate seed [10], *Rosa canina* sp. Seed [11], rubber seed [12] and safflower seed [13], etc.

In the AC production, various chemical activator agents have been used for the chemical activation of lignocellulosic materials; however, Zinc Chloride ($ZnCl_2$) offers various technical and economic advantages such as (i) its effectiveness to build up well developed microporous-mesoporous structure in the activated carbons (ACs); (ii) the production of ACs with high surface areas, considering low ratios of raw material/chemical activator and lower carbonization temperatures compared with others chemicals; (iii) high process yields; and, (iv) less expensive material [14, 15]. The most important disadvantage of all chemical activators is related to environmental concerns during the demineralization step. It has been reported [16] that in the case of cocoa pod husk-AC, the optimal condition in the activation with $ZnCl_2$ was when temperatures close to 600 °C where used, however temperatures higher than 700 °C had a negative effect on the AC properties.

Water pollution is a remarkable concern worldwide. However the amount of wastewater is increasing with the rapid growth of industrialization. The problems in Latin America related to water pollution are linked to organic and inorganic pollutants. Between organic contaminants, the occurrence of dyes in wastewaters is a significant problem, since many dyes are harmful for both humans and for the environment due to their toxicity. In fact, both the discharge volumes and wastewater compositions make wastewaters from textile industry the most polluting among all industrial sectors [17]. Between the most widely used dyes that could be in the content of the textile wastewater are methylene blue (MB), acid red 14, remazol red RR, reactive blue 19, methyl orange (MO), etc [18]. However previous works in water treatment have been used MB and MO as the most common models of dyes to be investigated [19].

In addition to that, one of the most important groups of inorganic pollutants is heavy metals and metalloids. Thus, drinking water sources contaminated by arsenic is a worldwide concern, considering the fact that it may occur naturally or as a consequence of human activities such as mining operations. Drinking water polluted by arsenic can cause serious health problems, such as skin lesions, hyperkeratosis and cancer [20].

This study aimed to use two renewable, low cost and up-to-now uninvestigated biomasses, *Spondias Purpurea L.* and *Inga Edulis* (Supporting Material - Fig. 1) as precursor to produce good quality $ZnCl_2$-based-ACs as potential adsorbents to be utilized in water treatment applications. The specific goals of this study are: (i) To determine textural, morphological, chemical and structural properties of two new raw agro-materials and correlate them with those of the produced ACs, (ii) to establish the relationship of the key AC properties with their adsorption capacity in kinetic experiments with MB, MO and As(V) as pollutants models; and (iii) to calculate the maximum adsorption capacity of MB and MO for the produced ACs using equilibrium experiments and compare them with those of others agro-waste ACs.

2 Material and methods

2.1 Raw materials

Samples of red mombin (*Spondias purpurea L.*) fruit and ice cream-bean (*Inga edulis*) were identified and collected from different agricultural areas in Tumbes, located in northwest Peru. Then the seeds were separated mechanically from the rest of the fruit and codified as RMS-RM and GS-RM for seeds from red mombin and ice cream-bean, respectively.

2.2 Chemicals

$ZnCl_2$ (Emsure ACS, ISO, Reag. Ph Eur - Merck) was used as activation agent to produce ACs. Methylene blue (Certistain C.I. 52015 - Merck) and Methyl Orange (Spectrum C.I. 13025 - USA) were used to prepare 1000 mg/L MB and MO stock solutions respectively for adsorption experiments. Sodium arsenate dibasic heptahydrate ($HAsNa_2O_4.7H_2O$, Sigma-Aldrich) was used for preparing a 100 mg/L As(V) stock solution for adsorption experiments. The As(V) stock solution was preserved with ultrapure concentrated (65 %) nitric acid (HNO_3) in order to have a final acid concentration of 0.2 % in the solution.

2.3 Characterization of raw agro-materials

The moisture content expressed in weight percentage (wt.%) of the precursors was determined using the oven-drying test method at 150 °C until constant weight was reached. After the water content was eliminated from the precursors, the ash content (wt.%) was calculated using the Muffle Furnace test method at 650 °C until constant weight was reached as well.

The bulk density, ρ_{Hg}, the skeletal density, $\rho_{He,}$ the porosity, ε, and the intrusion pore volume, $V_{intruse}$, of the processed raw agro-materials were determined by high-pressure mercury porosimetry and helium pycnometry measurements. Those measurements were conducted on an AutoPoreIII mercury porosimeter (Micromeritics, USA) and an AccuPycII1340 pycnometer (Micromeritics, USA). Before the measurements, the raw materials received as non-crushed seeds were dried in an oven at 105 °C for several days to remove the physisorbed moisture. For each precursor the high-pressure mercury porosimetry measurement was carried out at least twice in order to evaluate the average value of porosity because of the inhomogeneity in the pore structure of the raw materials. Porosity, ε (%), was calculated according to the following equation:

$$\varepsilon=(1-\rho_{Hg}/\rho_{He})*100. \quad (1),$$

The porous structure morphology of the raw agro-materials was observed using a field emission scanning electron microscope (FESEM) ZEISS ULTRA plus.

The elemental surface composition of the raw materials was conducted with a scanning electron microscope Tescan Indusem equipped with an energy dispersive spectroscopy (EDX) probe Bruker Quantax 125eV. A representative sample was taken from each raw material stock and the EDX analyses were done in three different areas of it. The averages of the measurements were reported.

2.4 Production of activated carbon

Non crushed RMS-RM was washed repeatedly in order to remove the remnant of fruit pulp and to avoid undesirable reactions during the activation and pyrolysis. GS-RM was used without being

washed because this material was able to be removed totally clean from the bean. Both seed samples were dried at 100 °C until constant weight, then they were ground and sieved to obtain the particle size fraction of 0.5–1 mm. $ZnCl_2$ was mixed with the sieved raw materials in a 1/1 weight proportion without addition of water. The ratio 1/1 raw material/$ZnCl_2$ has been reported by others authors as an effective ratio for agrowastes based-AC production [15, 16]; higher ratios could involve problems during activation and wash step and affect the final quality of ACs [21].

The raw materials with the activator agent were put in a metallic reactor and pyrolyzed at 600 °C during 2 h., using a heating rate of 10 °C/min. Then, an air flow was applied over the reactor to cool the samples down. The whole process of carbonization was conducted under a flux of nitrogen gas of around 150 mL/min. After the pyrolysis, the produced ACs were washed with a 0.15 M HCl solution and then washed exhaustively [22]. Finally, all ACs were dried at 100 °C overnight, ground and sieved with a mesh of 0.25 mm grid-size.

ACs prepared from red mombin and ice cream bean seeds were codified as RMS-AC and GS-AC respectively.

A flow chart of the AC production process (Supporting Material - Fig. 2) was elaborated for each precursor, including different steps from the raw material collection until its transformation in AC. A gravimetric method was used to determine the loss of weight in each step using a precision scale and then calculated as wt.%. The final yield (wt.%) of the AC production was calculated by the following equation:

$$Yield\,, wt.\% = \frac{FW}{IW} \times 100 \qquad (2),$$

where FW is the final weight of the produced AC and IW is the initial raw material weight (before the addition of the chemical activation agent).

2.5 Characterization of activated carbons

Proximate, elemental surface composition, textural, structural and morphological analyses were carried out over the samples.

Proximate analysis consisted of moisture in (wt.%), dry matter (wt.%) and ash content (wt.%) determinations. The moisture content was determined using the ASTM D2867-04 method and for the ash content, the ASTM D2866-94 (reapproved 2004) method was performed. This method considers the calculation of the ash content in dry basis using calcination temperatures of 650 ± 25 °C during several hours until constant weight is reached. The difference between 100 % and the moisture content (wt.%) gave the dry matter content (wt.%).

Nitrogen physisorption was used in order to determine textural parameters of the produced ACs and evaluated according a previous work [22]. The nitrogen physisorption measurements at 77 K were performed on a Gemini VII 2390 surface area analyzer (Micromeritics, USA). The specific surface area, S_{BET}, was calculated according to the classical Brunauer–Emmett–Teller (BET) theory for the p/p_0 range between 0.05 and 0.25 [23]. Since the specific surface area, S_{BET}, is not a proper parameter in the case of mesoporous solids containing micropores [24], the mesopore surface area, S_{meso}, and the micropore volume, V_{micro}, were also evaluated based on the modified BET equation with the C_{modif} constant [25, 26]. The results from modified BET equation were additionally correlated with the results from t-plot method, using Lecloux-Pirard standard isotherm and considering estimated C_{modif}. The net pore volume, V_{net}, was determined from the nitrogen adsorption isotherm at maximum p/p_0 (~0.9900). The mesopore-size distribution was evaluated from the desorption branch of the nitrogen adsorption-desorption isotherm by the Barrett–Joyner–Halenda (BJH) method

[27] via the Roberts algorithm [28], using the carbon standard isotherm and the assumption of the slit-pore geometry.

The structure order of the produced ACs was studied by collecting Raman spectra by using a dispersive Nicolet Almega XR spectrometer equipped with Olympus BX 51 microscope. An excitation laser source (473 nm) with an incident power of 5 mW with 256 expositions with 0.5 s duration was used for collecting the spectra. The laser beam was focused to a spot of 0.6 mm in diameter. The incident energy was minimized to avoid thermal effects as a consequence of the laser irradiation. The spectral resolution of the apparatus was 1.93 cm^{-1} and it was calibrated using a crystalline silicon standard with line at 520 cm^{-1}. An aluminium substrate was used to place the samples on during the analysis. The Raman spectra were taken from several different places within each sample.

Additionally, the pore shape and pore morphology were studied using images from a FESEM Zeiss Ultra plus. The elemental surface composition was done with a scanning electron microscope Tescan Indusem equipped with an EDX probe Bruker Quantax 125eV. For every produced AC, a representative sample (0.25 mm particle size) was taken from the stock and the EDX analyses were done in three different areas of it. The averages of the results were reported.

The pH of point of zero charge (pH_{PZC}) was calculated using the drift pH method. A 0.01 M solution of KNO_3 was prepared and bubbled during 40 min with nitrogen; the 50 ml of the solution were put in different flasks and the pH level was modified to reach values between 3 and 10 (8 points). pH values were modified by the addition of 0.1 M NaOH and H_2SO_4 solutions. 0.1 g of the AC samples was put into each flask with KNO_3 solutions and they were shaken during 48 hours to reach the equilibrium. After that the AC particles were filtered and the final pH was measured. The pH_{PZC} was calculated from the interception between the curves $pH_{initial}$ vs pH_{final} and $pH_{initial}$ vs $pH_{initial}$. These calculations were done twice and the average is reported.

2.6 Adsorption experiments

2.6.1 Kinetic experiments

Kinetic adsorption experiments provide valuable information about the reaction pathway and about the mechanism of sorption process [29]. Besides, these kinds of experiments permit calculate the solute adsorption rate in turn controls the residence time of sorbate uptake at the solid-solution interface. Thus, we were able to infer the rate and the initial adsorption rate at which pollutants are removed from aqueous solution and correlate it with the pore structure of the produced AC to have valuable data in order to design proper sorption treatments. In that sense we selected MB, MO and arsenic (V) as pollutants models based on criteria such as organic and inorganic nature of the compounds, molecular size and their high incidence in the aqueous environments.

The pH level was directly measured in the MB and MO solutions (it was respectively 7.40 and 7.74) and it was not adjusted during experiments. The temperature was between 20 and 25 °C. . The As(V) experiments included a pH adjustment from the initial pH 3.3 to pH 6.

In the case of MB and MO, the AC load was 0.5 g/L and the initial dyes concentration was 50 mg/L in 150 ml batches. The suspensions were mixed on a magnetic stirrer during the experiments. Different aliquots were extracted at the beginning and at different times between 5 and 150 min and then filtered through paper filter Whatman 41.To eliminate the possible error of dye retention over the paper filter, 1 ml of the sample was disposal before to take the sample to be measured. The dyes concentrations were determined on a Spectroquant Pharo 300 UV-VIS spectrophotometer (Merck), using a wavelength of of 660 and 464 nm for MB and MO respectively.

In the case of As(V), the AC load was 0.5 g/L and the initial As(V) concentration was 100 µg/L in 200 mL batches. The suspensions were shaken with a mechanical shaker Certomat at 175 rpm for 4 h. Suspensions were taken periodically at certain time intervals until 240 min, filtered through 0.2 µm syringe filters and acidified with HNO_3 p.a. in order to maintain the preservability of the liquid aliquots. The As(V) concentration in liquid aliquots was analyzed using an inductively coupled plasma mass spectrometer X Series II QICP-MS (Thermo Fisher Scientific) with a detection limit of 0.25 µg/L.

A pseudo-second order kinetic model was applied to describe the MB, MO and As(V) adsorption data. The integrated form of that model can be written as follows [29]:

$$\frac{t}{q_t} = \frac{1}{K_2 q_e^2} + \frac{t}{q_e} \quad (3),$$

where t is the adsorption time (min), q_t is the amount of pollutants (adsorbates) adsorbed at time t (mg of adsorbate/g of AC), k_2 is the pseudo-second-order rate constant (g of adsorbent/mg of adsorbate·min) and q_e is the calculated equilibrium adsorption capacity (mg of adsorbate/g of AC). The initial adsorption rate as q_t/t approaches 0, h (mg of adsorbate/g of adsorbent·min) was calculated according $h=k_2.q_e^2$

The amount of MB, MO or As(V) adsorbed at time t were calculated by using the following mass balance equation:

$$q_t = \frac{(C_0 - C_t)V}{m_{AC}} \quad (4),$$

where C_0 is the initial concentration of MB, MO or As(V) and C_t is the MB, MO or As(V) concentration in solution at time t (mg/L). V is the total volume of solution (l) and m_{AC} is the mass of AC (g). The plot of t/q_t as a function of time was graphed for each AC and each adsorbate to evaluate the validity of the pseudo-second order kinetic model and to calculate the kinetic parameters.

2.6.2 Equilibrium experiments

For the equilibrium experiments, five different initial concentrations of MB and MO were prepared in the range between 40 and 120 mg/L. For each dye, 100 ml of solutions were put in a 250 ml flask and 50 mg of ACs (less than 0.25 mm particle size) was added. Samples were shaken at 180 rpm in an orbital shaker during 24 hours period of time at the constant temperature of 30±2 °C. That period of time was selected based on preliminary tests to be sure that the equilibrium state is reached. The MB and MO concentrations were determined on a Spectroquant Pharo 300 UV-VIS spectrophotometer (Merck), using wavelengths of 660 and 464 nm respectively.

The Langmuir model [30] was employed to evaluate the equilibrium adsorption data of the adsorbents. The linear Langmuir isotherm equation is represented by the following equation:

$$\frac{C_e}{q_e} = \frac{1}{K_L q_{\max}} + \frac{C_e}{q_{\max}} \quad (5),$$

where q_e is the amount of MB or MO adsorbed at equilibrium time (mg/g), C_e is the equilibrium concentration of the adsorbed dyes (mg/L), q_{max} and K_L are Langmuir constants related to maximum adsorption capacity (monolayer capacity) and energy of adsorption respectively.

The equilibrium adsorption uptakes of MB and MO on the adsorbents, q_e (mg/g) were calculated using the following equation:

$$q_e = \frac{(C_0 - C_e)V}{m_{AC}} \qquad (6),$$

Where C_0 (mg/L) and C_e (mg/L) are initial concentration of the dyes and the concentration of the dyes at equilibrium respectively. V (L) is the volume of the solution and m_{AC} (g) is the amount of AC added.

The Freundlich model [31] was used as well to evaluate the equilibrium data. The logarithmic form of Freundlich model is given by:

$$\log q_e = \log K_F + \frac{1}{n}\log C_e \qquad (7),$$

where K_F can be defined as an adsorption or distribution coefficient and represents the amount of adsorbate adsorbed on an adsorbent for a unit equilibrium concentration. The slope *1/n* is a measure of the adsorption intensity or surface heterogeneity.

Kinetic and equilibrium experiments were conducted by duplicate and the average was reported in the case of MB and MO.

3 Results and discussion

3.1 Characterization of raw agro-materials

The proximate analysis (Supporting Material - Table 1) reveals that the moisture and ash contents in RMS-RM are lower than in GS-RM. According to the elemental surface composition (Supporting Material - Table 1) the most abundant elements on the surface of the raw materials particles were C, O and N, however, there were also minor elements such as Na, Mg, Al, Si, P, S, Cl, P, Ca and Fe present. C and O appeared approximately in the same weight proportion in both raw materials. Both of these elements are the main constituents of carbonaceous compounds (cellulose, hemicellulose and lignin) within the structure of vegetal products. The comparable amount of C in both raw materials was also proved by elemental bulk analysis (Supporting Material - Table 2).

Na and Al are presented in the surface of RMS-RM, but not in the case of GS-RM. Zn was neither detected in the surface of RMS-RM nor in GS-RM; it is important to have a baseline, taking into account that the chemical activation agent used for the activation process is $ZnCl_2$.

Low ash content and high carbon content in the precursor are desirable in order to produce high quality ACs [32], which was the case with both the studied raw-materials. Different agricultural by-products (around 14) have been studied for the manufacture of granular AC [33] and found that all precursors exhibited low ash content between 0.2 and 2.9 wt.% and high C content between 47.3 and 54.4 wt.%, comparable with the findings in this study.

The results from high-pressure mercury porosimetry and helium pycnometry measurements (Supporting Material - Table 1) obtained for both raw materials reveal that GS-RM is markedly less porous precursor than RMS-RM. The porosity of GS-RM is very low (~2.5±1%) compared to RMS-RM which possesses porosity of ~44±5 %. On the other hand, the repeated analyses revealed that the poor porous structure of GS-RM (Fig. 1b) is more regular than of RMS-RM (Fig. 1a), and GS-RM comprises larger pores as well as smaller pores. The porous structure of RMS-RM is very irregular. However, the greater porosity of RMS-RM could be more advantageous for the chemical activation, since the activator can enter the internal porous structure of the raw matter particles with fewer difficulties during the activation step, leading to a better established microporous-mesoporous structure of RMS-AC after the carbonization.

The FESEM micrographs, showing the morphology of both RMS-RM (Fig. 1c) and GS-RM (Fig. 1d), indicate that RMS-RM constitutes of layers/slices, while the structure of GS-RM is compact with an irregular surface. Either of the raw materials do not show highly porous structure.

RMS-RM was markedly more porous (~44±5 %) than GS-RM (~2.5±1 %), but GS-RM exhibited more homogeneous porous structure. Both precursors exhibited low ash contents and high carbon contents, comparable with those of others precursor.

3.2 Characterization of produced activated carbons

The elemental surface composition (Supporting Material - Table 3) revealed that C is the main component in both ACs, followed by O and the others minor elements. Comparing the precursors and the produced ACs, the C/O proportion was different. Since the carbonization process involves the release of CO_2, the content of O (%) decreases and the content of C (%) increases during that step.

The percentage of Cl increases in the case of both ACs surface in relation to the starting materials. Zn appeared in both adsorbent materials; however, in the raw materials it is not present. Both elements remain as residues in the prepared ACs from the chemical activator.

The ash content in RMS-AC (38.8 wt.% in dry basis) was significantly higher than in GS-AC (10.0 wt.% in dry basis). The presence of minor elements such as Na, Mg, Al, Si, Ca and Fe in the RMS-RM, is one of the reasons for the high ash content in RMS-AC. Another reason is the remaining chemical activator in the AC. High ash content in the ACs could affect negatively their textural properties, reducing their adsorption capacity. However, high ash contents in ACs produced from agricultural wastes, as high as in the case of RMS-AC, has been reported in others studies for adsorption in aqueous solutions [15].

The nitrogen adsorption-desorption isotherms measured for the produced ACs and pore-size distributions are shown in Fig. 2. The evaluated textural parameters of both produced ACs are summarized in the Supporting Material - Table 3.

It is evident that both produced adsorbents exhibit microporous-mesoporous structure. The shape of nitrogen adsorption-desorption isotherms (Fig. 2a) corresponds basically to the type I isotherm according to the IUPAC classification [24], typical for microporous materials. Besides, the isotherms include hysteresis loops at higher relative pressures, which are typical for the type IV IUPAC isotherm, indicating the presence of some mesopores. Features of nitrogen adsorption-desorption isotherms correspond pretty well to the evaluated pore-size distributions shown in Fig. 2b, evaluated for the slit-pore geometry of mesopores. It can be seen that the microporous-mesoporous structure is well established in both adsorbents, but RMS-AC possesses significantly higher mesopore surface area (about ~200 m^2/g) and volume of micropores (about ~132 mm^3_{liq}/g) than GS-AC. Concerning the mesopore sizes, GS-AC includes a bit wider mesopores than RMS-AC. These features could contribute to the explanation of sorption abilities of RMS-AC and GC-AC.

RMS-AC and GC-AC exhibited high S_{BET}, 1405 and 937 m^2/g, respectively. The Supporting Material - Table 4 shows a comparison between S_{BET} of the ACs from both raw materials used in this study and those from different seeds-ACs. From the comparison it can be seen that the ACs produced in this study possess comparable surface area levels than those ACs prepared similarly (by $ZnCl_2$ activation, carbonization at 600°C) but from others types of seeds. Pereira et al. [34] produced $ZnCl_2$-AC from red mombin seed for food application with high S_{BET} = 956 m^2/g. However the S_{BET} found in the present study is still higher. It is based on the different production parameters. Longer carbonization time, higher temperature and higher $ZnCl_2$/precursor ratio were determining to produce RMS-AC with higher S_{BET} and possibly with different pore structure.

The Raman spectra, characterizing the structure of GS-AC and RMS-AC (Fig. 2c), have two broad bands centered at 1358 cm^{-1} (D-band) and 1609 cm^{-1} (G-band), and 1367 cm^{-1} and 1607 cm^{-1}, respectively. The full width at half maximum (FWHM) of the G-band corresponding to RMS-AC and GS-AC is 69 cm^{-1} and 77 cm^{-1}, respectively. It can be deduced, from the dependence of G-FWHM on interlayer spacing of carbon films [35], that d_{002} values of the ACs are greater than 0.343 nm which proves the presence of the turbostratic carbon forms in the produced ACs.

The carbonization of both the raw materials was accomplished at relatively low temperature (600 °C) and the amorphous character of the prepared carbon is dominating above the nanocrystalline forms. In both ACs, the G peak positions above 1600 cm^{-1} give an evidence for a low hydrogen content (lower than 20 at.%). In addition, the C-H bonding vibration region (above 3000 cm^{-1}) gives no feature showing the presence of C-H bonds. In this region only the second order of the G band (2G) is located at 3206 and 3202 cm^{-1}, G+D combination vibrations centered at around 2950-2960 cm^{-1} and a broad bump corresponding to 2D vibrations appears between 2300 and 3200 cm^{-1}.

The G-band widths for RMS-AC and GS-AC are 69 and 77 cm^{-1}, respectively. The corresponding I_D/I_G ratios are 1.61 (RMS-AC) and 1.52 (GS-AC), which means that the cluster sizes are smaller than 1 nm according to the Tuinstra and Koenig equation [36].

The produced ACs possess a developed macroporous structure (Supporting Material - Fig. 3) compared to the raw materials (Fig. 1c and 1d). In most cases, the macropores of both ACs have an irregular shape, they are not perfectly circular. The macropores of RMS-AC (Supporting Material - Fig. 3a and 3b) are cleaner and show more homogeneous and regular distribution compared to the GS-AC sample (Supporting Material - Fig. 3c and 3d). Some impurities on the surface of the ACs were detected in the FESEM pictures. These impurities might be from the chemical activator (Zn and Cl) and different pyrolysis by-products or residues generated during the final grinding step.

The activated carbons from both raw materials have well-established microporous-mesoporous structure, but RMS-AC exhibits higher mesopore surface area, micropore volume as well as net pore volume (S_{BET} of 1405 m^2/g, S_{meso} of 965 m^2/g, V_{micro} of 214 mm^3_{liq}/g, V_{net} of 792 mm^3_{liq}/g) than GS-AC. Concerning the mesopore sizes, GS-AC has a bit wider mesopores than RMS-AC. The presence of minor compounds (Na, Mg, Al, Si, Ca and Fe) in the red mombin seed (RMS-RM) contributed to the high ash content in the produced activated carbon (RMS-AC).

3.3 Adsorption experiments

3.3.1 Kinetic experiments

Fig. 3(a,b,c) shows the removal of MB, MO and As(V) as functions of time for both produced ACs. Both ACs are able to adsorb efficiently MB, reaching comparable removal levels, over 90 % after 1h. Levels of MO removal are high as well; nevertheless the highest levels are reached after 100 min. The As(V) adsorption performances of individual produced ACs are quite different, significantly higher for RMS-AC.

In spite of the fact that porous structure is well established in both produced ACs according to physisorption measurements and FESEM, the wider mesopores in GS-AC enable MB molecules to be transported and adsorbed more effectively on the surface of micropores and mesopores than in pores of RMS-AC. Therefore, the MB adsorption during the first 30 min, when the diffusion of MB molecules into AC porous structure plays a dominant role, is higher for GS-AC (the pores of GS-AC are rather accessible). Nevertheless, after 1 h, when the adsorption equilibrium is reached, the RMS-AC exhibits higher adsorption capacity due to a generally larger surface area. Moreover, considering the molecular dimension of MB 1.7 x 0.76 x 0.33 nm [37], it can be reasonably supposed that the adsorption of MB cannot occur on the whole micropore surface of both ACs. Thus, in the case of MB

adsorption, the mesopore surface area will be a more important (determining) parameter than the microporosity.

Since the methyl orange molecular size is 1.19 x 0.67 x 0.38 nm [38] similar phenomena occurred. ´Pore size distribution of ACs plays the determining role during the uptake process. GS-AC showed better adsorption removal of MO during the first 30 min, while RMS-AC overcomes the MO adsorption capacity of GS-AC after 30 min to the final of the experiment.

It is very interesting that both ACs present the ability to adsorb both MB and MO, two dyes with opposite nature: cationic/basic and anionic/acid respectively. Taking into account that (i) the pH of the solution during the experiments (Fig. 3d and 3e) was not so different than neutral level, (ii) the pH of the solution was close to the pH_{PZC} of the ACs (6.8±0.1 and 7.2±0.1 for GS-AC and RMS-AC respectively) and (iii) MB and MO are organic molecules with high molecular size, the electrostatic interactions between the adsorbate and adsorbent were minimal during the adsorption experiments. Conversely, the dispersion interactions (non-electrostatic interactions) were maximal. The non-electrostatic interactions are always attractive, and can include van der Waals forces, hydrophobic interactions and hydrogen bonding [39]. Therefore the MB and MO adsorption depends on mesoporous surface area (2-50 nm pore size).

The As(V) adsorption capacity for RMS-AC is higher than for GS-AC (Fig. 3c). The As(V) removal for RMS-AC reached a level close to 100 % after 2 h. In the case of GS-AC the maximum As(V) removal capacity level is close to 60 % after 2 h. Around pH 6 (see the evolution of the pH during the experiments in the Fig. 3f), As(V) exists predominantly as arsenate species $H_2AsO_4^-$, and its molecular size is 0.38 nm on average [40]. It means that in the case of As(V) removal, the AC porous structure (including micropores) does not limit the transport and adsorption of this small molecular size pollutant to the whole surface area. Besides ACs surface area and pore-size distribution, there are others factors that may influence the metallic ions adsorption on ACs: the metal ion speciation or metal ion complex, the solution pH, the pH_{PZC} of ACs and the functional groups on the ACs surface [41].

Comparing the evolution of the pH values during the As adsorption experiments and the pH_{PZC} of both ACs (mentioned above) it is possible to infer that the net charge of the ACs surface is positive because the pH_{PZC} of the samples was higher than the solution pH through the time. Considering that As(V) at that pH solution levels is present as oxyanion charged negatively both ACs would be the ability to adsorb arsenic in solution at the experimental conditions.

Various authors [42] [43] have found that carbons with higher ash content are more suitable to adsorb As(V), being a parameter even more important than the specific surface area. The relationship between both parameters the ash content and As(V) adsorption is direct, being RMS-AC the sample with higher ash content (38 wt.%) and with better As(V) adsorption capacity, while GS-AC with lower ash content (10 wt.%) exhibits less As(V) adsorption capacity.

The time dependences of MB, MO and As(V) removal of the produced ACs were fitted with a pseudo-second order kinetic model and the t/q_t as a function of time give a linear correlation with all the experimental measurements. The fact that the prepared ACs perfectly follow this model, revealed that the type of adsorption between adsorbate and adsorbent is chemical. The kinetic parameters for MB, MO and As(V) adsorption, k_2 and q_e, were obtained from the slope and the intercept of the graphs t/q_t as a function of time and are presented in the Supporting Material - Table 5.

In the case of MB, the calculated equilibrium adsorption capacity (q_e) for RMS-AC (105.3 mg/g) was higher than for GS-AC (98.1 mg/g) coinciding with the higher surface area in the first AC. The higher pseudo-second-order rate constant (k_2) in the case of GS-AC (0.0022 g/mg·min) compared with of RMS-AC (0.0013 g/mg·min), reveals that GS-AC reached its respective q_e more quickly than RMS-AC, nevertheless q_e of GS-AC is lower than of RMS-AC. The correlation coefficients R^2 (0.997-0.999)

indicate that the adsorption data of both samples fits pretty well to the pseudo-second kinetic model.

The tendency of the MO kinetic adsorption parameters was similar as for MB comparing both ACs: q_e values were 106.38 and 97.09 mg/g for each AC, K_2 =0.006 and 0.0012 g/mg·min, h =7.3 and 11.0 and R^2 =0.990 and 0.993 for RMS-AC and GS-AC respectively.

Concerning As(V) adsorption, both ACs fit pretty well with the pseudo-second order kinetic model (R^2=0.997 and 0.996 for RMS-AC and GS-AC, respectively). While RMS-AC exhibits higher q_e (0.22 mg/g) than GS-AC (0.15 mg/g), it shows lower k_2 (0.4050 g/mg·min) than GS-AC (0.5910 g/mg·min). RMS-AC has higher adsorption performance for As(V) uptake according to the kinetic parameters, however, in this case the microporosity, surface area and pore structure morphology might not be limiting factors for the adsorption of As(V). Whereas, in As(V) case, supported by the literature, the higher ash content may be one of the parameters having strong influence on As(V) adsorption.

Analyzing the initial adsorption rates (h) for MB and MO uptakes, they are higher for GS-AC (21.0 and 11.0 mg/g·min) than for RMS-AC (14.9 and 7.3 mg/g·min). This fact is in line with the better MB and MO adsorption performance of GS-AC during the first 30 min, because of the wider mesopores as discussed above. In the case of As(V) adsorption, RMS-AC exhibited higher h (0.0198 mg/g·min) than GS-AC (0.0126 mg/g·min), corresponding with better initial adsorption performance of the As(V) adsorption.

Both activated carbons have the ability to adsorb MB, MO and As(V) in aqueous solutions during kinetic experiments and the kinetic adsorption data in all cases fitted pretty well fitted to a pseudo-second order kinetic model (R^2>0.99). This fact suggests chemical adsorption between the adsorbates and the activated carbons.

3.3.2 Equilibirum experiments

The MB and MO equilibrium adsorption data of the produced ACs fitted better to the Langmuir equilibrium model than to the Freundlich model. The isotherms of the both models are exhibited in the Supporting Material - Fig. 4a and 4b for MB and the Supporting Material - Fig. 4d and 4e for MO. All values of R^2 were higher than 0.99 (Supporting Material - Table 5) supposing that the adsorption process between MB or MO and the produced ACs is homogeneous in the monolayer.

According the Langmuir model the maximum MB adsorption in the equilibrium state (q_{max}) was 222.2 mg/g for RMS-AC and 204.1 mg/g for GS-AC. It is in accordance with the kinetic experiments and the fact that mainly the mesopore surface area is the key adsorption factor for the higher maximum MB adsorption by RMS-AC. Rafatullah et al. [44] compared the MB adsorption capacity of 49 different low cost ACs (made of industrial and agricultural wastes), finding MB adsorption capacities between 0.84 to 486 mg/g. The results of this study are at least in the middle of the mentioned range comparable with olive-seed waste residue-based activated carbon (190–263 mg/g), AC prepared from oil palm shell (243.90 mg/g), *Hevea brasiliensis* seed coat-AC (227.27 mg/g) and jute fiber carbon (225.64 mg/g).

Whereas the MO maximum adsorption in the equilibrium state (q_{max}) was 208.3 mg/g for RMS-AC and 172.4 mg/g for GS-AC. The figure is the same that in the case of MB, the higher mesopore surface area, the higher maximum MO adsorption capacity.

The Supporting Material - Fig. 4c and 4f presents the relationship between the initial concentration (C_0) and the adsorbed amount of MB and MO on the solid phase (q_e). The higher C_0, the higher q_e. According to Cherifi et al. [45] it is based on the fact that the initial concentration of MB or MO

provided an important driving force to overcome all mass transfer resistance and the interaction between MB or MO and AC increased.

Regards to MB and MO adsorption, the specific surface area and the pore size distribution of the produced ACs play an important role, while for As(V) uptake, the ash content in the ACs might play a determining role in its adsorption. The maximum MB adsorption capacity by the activated carbons was 222.2 and 204.1 mg/g respectively, levels comparable with others agro-waste based activated carbons.

4 Conclusions

Seeds from *Spondias purpurea* L. (red mombin) and *Inga edulis* (ice cream beam), RMS-RM and GS-RM, respectively, were tested as unconventional precursors to produce activated carbons for potential applications in water and/or wastewater treatment.

RMS-RM was markedly more porous (~44±5 %) than GS-RM (~2.5±1 %), but GS-RM exhibited more homogeneous porous structure. Both precursors exhibited low ash contents and high carbon contents, comparable with those of others precursors. The activated carbons from both raw materials have well-established microporous-mesoporous structure, but RMS-AC exhibits higher mesopore surface area, micropore volume as well as net pore volume (S_{BET} of 1405 m^2/g, S_{meso} of 965 m^2/g, V_{micro} of 214 mm^3_{liq}/g, V_{net} of 792 mm^3_{liq}/g) than GS-AC. Concerning the mesopore sizes, GS-AC has a bit wider mesopores than RMS-AC. The presence of minor compounds (Na, Mg, Al, Si, Ca and Fe) in the red mombin seed (RMS-RM) contributed to the high ash content in the produced activated carbon (RMS-AC).

Both activated carbons have the ability to adsorb MB, MO and As(V) in aqueous solutions during kinetic experiments and the kinetic adsorption data in all cases fitted pretty well fitted to a pseudo-second order kinetic model (R^2>0.99). This fact suggests chemical adsorption between the adsorbates and the activated carbons.

Regards to MB and MO adsorption, the specific surface area and the pore size distribution of the produced ACs play an important role, while for As(V) uptake, the ash content in the ACs might play a determining role in its adsorption.

The maximum MB adsorption capacity by the activated carbons was 222.2 and 204.1 mg/g respectively, levels comparable with others agro-waste based activated carbons.

Seeds from red mombin and ice cream bean can be definitely considered as unconventional, cheap and suitable raw materials for production of $ZnCl_2$ activated carbons of good adsorption properties to be used in water or wastewater treatment.

Compliance with ethical standards

Funding and acknowledgement

The National University of Tumbes provided important financial support (Proyecto Canon – Resolución N° 0722-2014/UNT-R). The Academy of Sciences of the Czech Republic and Consejo Nacional de Ciencia, Tecnologia e Innovación Tecnológica (CONCYTEC) in Peru (joint project reg. No. 002/PE/2012) are gratefully recognized for their support. The Academy of Finland is acknowledged for research funding to the AdMatU project (DNo: 269631) from the Development funds. The Finnish Funding Agency for Technology and Innovation (Tekes) is acknowledged for the funding of HYMEPRO–project (DNo: 845/31/2011). The authors are very grateful to John Rimaycuna for his technical support.

List of Symbols

C_0 initial concentration of adsorbate in solution (mg/l)

C_e equilibrium concentration of the solute (mg/l)

C_{modif} adsorption constant in the first layer calculated according to the modified BET equation (-)

C_t adsorbate concentration in solution at time t (mg/l)

GS-AC *Inga edulis* (ice cream-bean) seed derived activated carbon

GS-RM *Inga edulis* (ice cream-bean) seed

h initial adsorption rate as q_t/t approaches 0 (mg/g·min)

k_2 pseudo-second-order rate constant (g/mg·min)

K_F Freundlich constant related to the degree of adsorption

K_L Langmuir constant (l/g)

m_{AC} mass of activated carbon (g)

n Freundlich constant related to intensity of the adsorption

pH_{PZC} pH of point of zero charge

q_e calculated equilibrium adsorption capacity (mg/g)

q_{max} maximum adsorption in the equilibrium state (mg/g)

q_t amount adsorbed at time t (mg/g)

RMS-AC *Spondias purpurea* L. (red mombin) seed derived activated carbon

RMS-RM *Spondias purpurea* L. (red mombin) seed

S_{BET} specific surface area calculated according to the classical BET theory (m^2/g)

S_{meso} mesopore surface area calculated according to the modified BET equation (m^2/g)

t adsorption time (min)

V total volume of solution (l)

$V_{intruse}$ pore volume determined by high-pressure mercury intrusion (cm^3/g)

V_{micro} micropore volume calculated according to the modified BET equation (mm^3_{liq}/g)

V_{net} net pore volume determined from the nitrogen adsorption isotherm at maximum p/p_0~0.9900) (mm^3_{liq}/g)

ε porosity of the raw material (%)

$\rho_{He,}$ skeletal density of the raw material (g/cm^3)

ρ_{Hg} bulk density of the raw material (g/cm^3)

References

[1] C.W. Purnomo, C. Salim, H. Hinode, *J. Anal. Appl. Pyrol.*, **2011**, *91 (1)*, 257-262. DOI: 10.1016/j.jaap.2011.02.017

[2] M.J. Martin, A. Artola, M.D. Balaguer, M. Rigola, *Chem Eng J*, **2003**, *94 (3)*, 231-239. DOI: 10.1016/S1385-8947(03)00054-8

[3] B.S. Girgis, A.N.A. El-Hendawy, *Micropor. Mesopor. Mat.*, **2002**, *52 (2)*, 105-117. DOI: 10.1016/S1387-1811(01)00481-4

[4] L.A. Rodrigues, M.L.C.P. da Silva, M.O. Alvarez-Mendes, A.D. Coutinho, G.P. Thim, *Chem. Eng. J.*, **2011**, *174 (1)*, 49-57. DOI: 10.1016/j.cej.2011.08.027

[5] M. Olivares-Marin, C. Fernandez-Gonzalez, A. Macias-Garcia, V. Gomez-Serrano, *Appl. Surf. Sci.*, **2006**, *252 (17)*, 5967-5971. DOI: 10.1016/j.apsusc.2005.11.008

[6] I. Okman, S. Karagoz, T. Tay, M. Erdem, *Appl. Surf. Sci.*, **2014**, *293,* 138-142. DOI: 10.1016/j.apsusc.2013.12.117

[7] M. Al Bahri, L. Calvo, M.A. Gilarranz, J.J. Rodriguez, *Chem. Eng. J.*, **2012**, *203,* 348-356. DOI: 10.1016/j.cej.2012.07.053

[8] D. Angin, *Fuel*, **2014**, *115,* 804-811. 10.1016/j.fuel.2013.04.060

[9] I. Kula, M. Ugurlu, M.H. Karaoglu, A. Celik, *Bioresource Technol.*, **2008**, *99 (3)*, 492-501. DOI: 10.1016/j.biortech.2007.01.015

[10] S. Ucar, M. Erdem, T. Tay, S. Karagoz, *Appl. Surf. Sci.*, **2009**, *255 (21)*, 8890-8896. DOI: 10.1016/j.apsusc.2009.06.080

[11] A. Gurses, C. Dogar, S. Karaca, M. Acikyildiz, R. Bayrak, *J. Hazard. Mater.*, **2006**, *131 (1-3)*, 254-259. DOI: 10.1016/j.jhazmat.2005.09.014

[12] K. Sun, J.C. Jiang, *Biomass Bioenerg*, **2010**, *34 (4)*, 539-544. DOI: 10.1016/j.biombioe.2009.12.020

[13] D. Angin, T.E. Kose, U. Selengil, *Appl. Surf. Sci.*, **2013**, *280,* 705-710. DOI: 10.1016/j.apsusc.2013.05.046

[14] J.A. Yang, K.Q. Qiu, *Chem Eng J*, **2011**, *167 (1)*, 148-154. DOI: 10.1016/j.cej.2010.12.013

[15] D. Kalderis, S. Bethanis, P. Paraskeva, E. Diamadopoulos, *Bioresource Technol.*, **2008**, *99 (15)*, 6809-6816. DOI: 10.1016/j.biortech.2008.01.041

[16] G. Cruz, M. Pirilä, M. Huuhtanen, L. Carrión, E. Alvarenga, R.L. Keiski, *Journal of Civil & Environmental Engineering*, **2012**, *2,* 1-6. DOI: 10.4172/2165-784X.1000109

[17] A.R. Tehrani-Bagha, N.M. Mahmoodi, F.M. Menger, *Desalination*, **2010**, *260 (1-3)*, 34-38. DOI: 10.1016/j.desal.2010.05.004

[18] R. Saravanan, S. Karthikeyan, V.K. Gupta, G. Sekaran, V. Narayanan, A. Stephen, *Mat. Sci. Eng. C-Mater.*, **2013**, *33 (1)*, 91-98. DOI: 10.1016/j.msec.2012.08.011

[19] R. Saravanan, M.M. Khan, V.K. Gupta, E. Mosquera, F. Gracia, V. Narayanan, A. Stephen, *J. Colloid Interf. Sci.*, **2015**, *452,* 126-133. DOI: 10.1016/j.jcis.2015.04.035

[20] T. Yoshida, H. Yamauchi, G.F. Sun, *Toxicol. Appl. Pharm.*, **2004**, *198 (3)*, 243-252. DOI: 10.1016/j.taap.2003.10.002

[21] A. Ahmadpour, D.D. Do, *Carbon*, **1997**, *35 (12)*, 1723-1732. DOI: 10.1016/S0008-6223(97)00127-9

[22] G.J.F. Cruz, L. Matejova, M. Pirila, K. Ainassaari, C.A. Canepa, J. Solis, J.F. Cruz, O. Solcova, R.L. Keiski, *Water Air Soil Poll.*, **2015**, *226 (11)*. DOI: 10.1007/s11270-015-2540-1

[23] S. Brunauer, P.H. Emmett, E. Teller, *J. Am. Chem. Soc.*, **1938**, *60 (2)*, 309-319.

[24] S.J. Gregg, K.S.W. Sing, Adsorption. Surface Area and Porosity, Academic Press, New York, **1982**.

[25] P. Schneider, *Appl. Catal., A*, **1995**, *129 (2)*, 157-165. DOI: 10.1016/0926-860x(95)00110-7

[26] A. Lecloux, J.P. Pirard, *J. Colloid Interf. Sci.*, **1979**, *70 (2)*, 265-281. DOI: 10.1016/0021-9797(79)90031-6

[27] E.P. Barrett, L.G. Joyner, P.P. Halenda, *J. Am. Chem. Soc.*, **1951**, *73 (1)*, 373-380. DOI: 10.1021/ja01145a126

[28] B.F. Roberts, *J. Colloid Interface Sci.*, **1967**, *23 (2)*, 266-273.

[29] Y.S. Ho,G. McKay, *Process Biochem.*, **1999**,*34 (5)*, 451-465. DOI: 10.1016/S0032-9592(98)00112-5

[30] I. Langmuir, *J. Am. Chem. Soc.*, **1918**, *40 (9)*, 1361-1403. DOI: 10.1021/ja02242a004

[31] H.M.F. Freundlich, *J. Chem..Phys.*, **1906**, *57,* 385-470.

[32] A.C. Lua, T. Yang, *J. Colloid Interf. Sci.*, **2004**, *274 (2)*, 594-601. DOI: 10.1016/j.jcis.2003.10.001

[33] W. Heschel, E. Klose, *Fuel*, **1995**, *74 (12)*, 1786-1791. DOI: 10.1016/0016-2361(95)80009-7

[34] R.G. Pereira, C.M. Veloso, N.M. da Silva, L.F. de Sousa, R.C.F. Bonomo, A.O. de Souza, M.O.D. Souza, R.D.I. Fontan, *Fuel Process. Technol.*, **2014**, *126,* 476-486. DOI: 10.1016/j.fuproc.2014.06.001

[35] A. Yoshida, Y. Kaburagi, Y. Hishiyama, *Carbon*, **2006**, *44 (11)*, 2333-2335. DOI: 10.1016/j.carbon.2006.05.020

[36] F. Tuinstra, J.L. Koenig, *J. Chem. Phys.*, **1970**, *53 (3)*, 1126-&. DOI: 10.1063/1.1674108

[37] Y. Umemura, E. Shinohara, R.A. Schoonheydt, *Phys. Chem. Chem. Phys.*, **2009**, *11 (42)*, 9804-9810. DOI: 10.1039/b817635c

[38] J.H. Huang, K.L. Huang, S.Q. Liu, A.T. Wang, C. Yan, *Colloid Surface A*, **2008**, *330 (1)*, 55-61. DOI: 10.1016/j.colsurfa.2008.07.050

[39] C. Moreno-Castilla, *Carbon*, **2004**, *42 (1)*, 83-94. DOI: 10.1016/j.carbon.2003.09.022

[40] T. Urase, J. Oh, K. Yamamoto, *Desalination*, **1998**, *117 (1-3)*, 11-18. DOI: 10.1016/S0011-9164(98)00062-9

[41] J.M. Dias, M.C.M. Alvim-Ferraz, M.F. Almeida, J. Rivera-Utrilla, M. Sanchez-Polo, *J. Environ. Manage.*, **2007**, *85 (4)*, 833-846. DOI: 10.1016/j.jenvman.2007.07.031

[42] L. Lorenzen, J.S.J. Vandeventer, W.M. Landi, *Miner. Eng.*, **1995**, *8 (4-5)*, 557-569. DOI: 10.1016/0892-6875(95)00017-K

[43] E. Diamadopoulos, P. Samaras, G.P. Sakellaropoulos, *Water Sci. Technol.*, **1992**, *25 (1)*, 153-160.

[44] M. Rafatullah, O. Sulaiman, R. Hashim, A. Ahmad, *J. Hazard. Mater.*, **2010**, *177 (1-3)*, 70-80. DOI: 10.1016/j.jhazmat.2009.12.047

[45] H. Cherifi, B. Fatiha, H. Salah, *Appl. Surf. Sci.*, **2013**, *282,* 52-59. DOI: 10.1016/j.apsusc.2013.05.031

[46] M. Pirila, Adsorption and photocatalysis in water treatment – Active, abundant and inexpensive materials and methods, Faculty of Technology, University of Oulu, Oulu, Finland, **2015**.

Figure captions

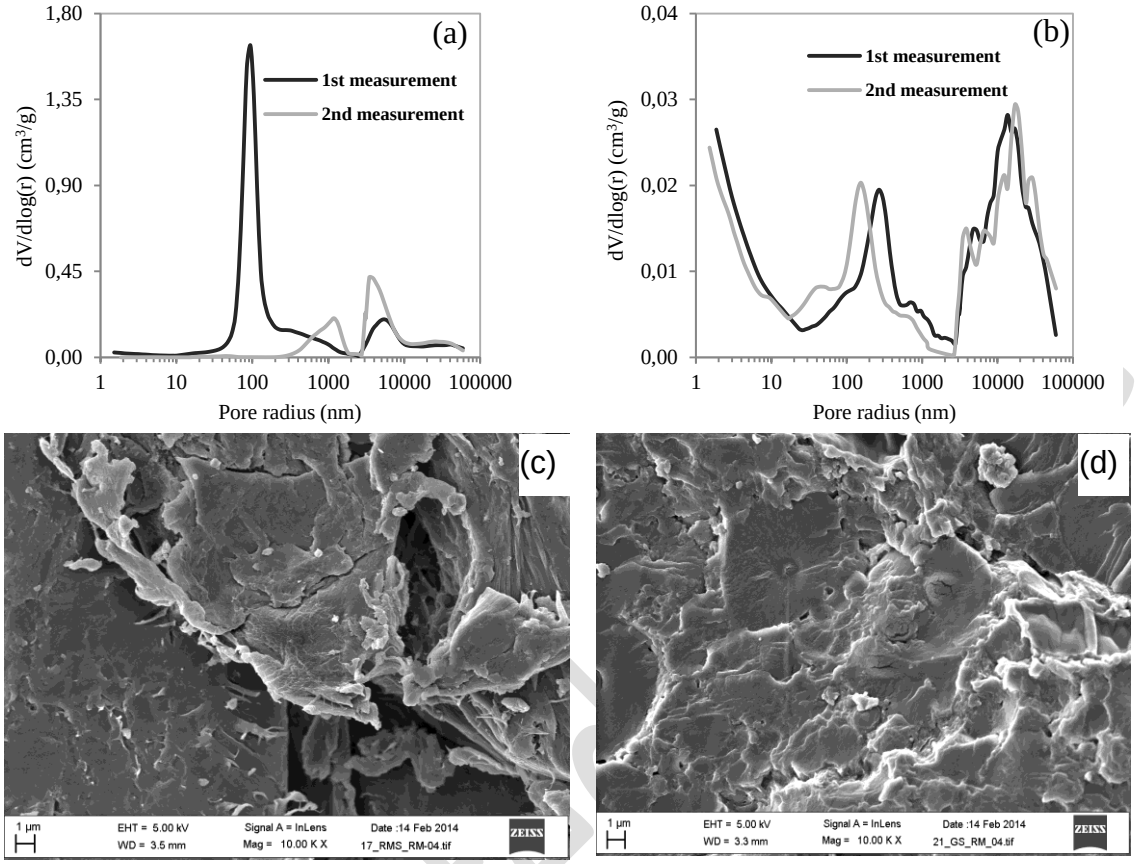

Fig. 1 Pore size distribution and FESEM micrographs of both raw materials RMS-RM (a,c) and GS-RM (b,d) [46].

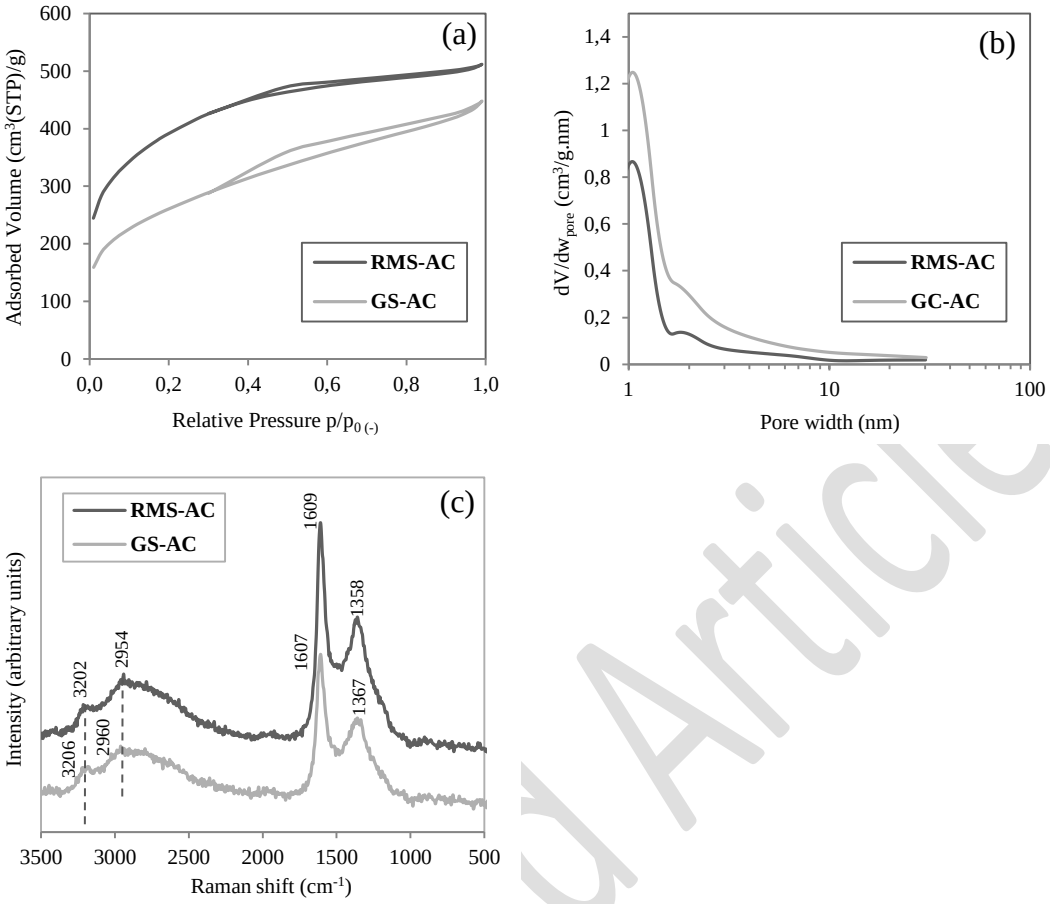

Fig. 2 Measured nitrogen adsorption-desorption isotherms (a), evaluated pore-size distributions (b) and Raman spectra (c) of the produced ACs [46].

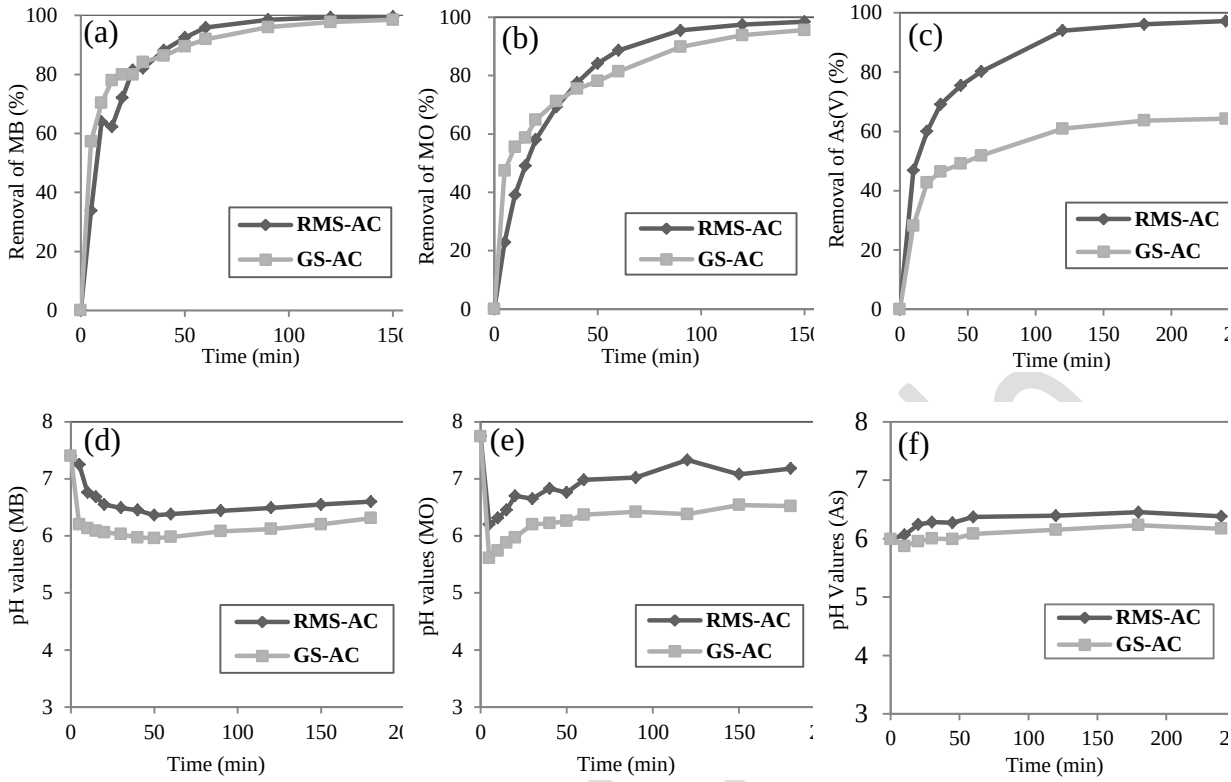

Fig. 3 Removal of MB (a) MO (b) and As(V) (c) using the produced ACs (MB and MO initial concentration=50 mg/L, As initial concentration=100 µg/L, AC load=0.5 g/L) with their respective pH values during kinetic experiments (d,e,f).

Short text to attract readers

Two unconventional precursors were used to prepared $ZnCl_2$-activated carbons with well-developed microporous-mesoporous structures. Activated carbons showed excellent adsorption performance for MB, MO as well as As(V). Dispersion interaction was the limiting factor during MB and MO adsorption.